Entrainment and deposition of boulders in a gravel bed river

Pascal Allemand[1], Eric Lajeunesse[2], Olivier Devauchelle[2], Vincent J. Langlois[1]

[1]Université Claude Bernard Lyon 1, ENS Lyon, Université Jean Monnet Saint-Étienne & CNRS, Laboratoire de Géologie de Lyon, Terre Planètes Environnement, UMR 5276, 69100 Villeurbanne, France

[2]Université de Paris, Institut de Physique du Globe de Paris, CNRS, F-75005, Paris, France

Correspondence to: Pascal Allemand (allemand@univ-lyon1.fr)

Abstract.

~~We~~Bedload transport, entrainment of coarse sediment by a river, is inherently a stochastic and intermittent process whose monitoring remains challenging. Here, we propose a new method to characterize bedload transport in ~~rivers~~the field. Using ~~a drone~~an Uncrewed Aerial Vehicle (UAV) equipped with a high resolution camera, we recorded yearly images of a bar of the Vieux-Habitants river, a gravel-bed river located on Basse-Terre Island (Guadeloupe, French West Indies). These images, combined with high frequency measurements of the river discharge, allow us to monitor the evolution of the population of ~~boulders~~ sediments of diameter between 0.5 and 0.75 m on the river bed. Based on this dataset, we estimate the smallest discharge that can move ~~the~~these boulders~~,~~ and calculate the ~~time during which the river effectively transports them~~duration of effective transport. We find that the transport of boulders occurs for approximately 10 hours per year. When plotted as a function of the effective transport time, ~~the~~a given population of boulders ~~that were in place at the beginning of the survey~~ decreases exponentially~~,~~ with an effective residence time of approximately 17 hours. ~~Based on our results, we suggest a new method~~This exponential decay suggests that the probability to ~~estimate~~ dislodge a grain from the bed is proportional to the number of grains at repose on the bed, an observation consistent with laboratory experiments. Finally, the residence time of bedload particles on a river bed can be used to evaluate bedload discharge~~ in gravel bed rivers~~.

1 Introduction

Rivers collect sediment from the surrounding hillslopes and carry it ~~down~~ to the ~~oceans~~ocean (Leopold and Emmett, 1976). The ~~resulting~~resultant sediment ~~flux~~discharge is often intermittent: only during floods does the river exert a force strong enough to move the sediments ~~of~~that make up its bed (Phillips and Jerolmack, 2014; Philipps et al., 2018). Flood after flood, a river gradually exports sediment ~~out of~~from its catchment. The frequency of ~~the~~ floods and the quantity of sediment that ~~each of them~~it transports thus set the erosion rate within the catchment (Wolman and Miller, 1960).

The fate of a particle entrained during a flood depends on its size. Fine sediments are often carried in suspension. ~~Coarse~~In contrast, coarse sediments~~, conversely,~~ travel as bedload: they roll, slip and bounce on the river bed, until ~~they~~motion

1

eventually ~~ceases and the grains~~ settle ~~down~~at a downstream location. This process is inherently stochastic (Einstein, 1937).

A turbulent burst or a collision with a travelling grain can dislodge a particle from the bed (Charru et al., 2004; Ancey et al., 2008; Houssais and Lajeunesse, 2012). Once in motion, the particle's velocity fluctuates and its eventual deposition is, again, a random process (Lajeunesse et al., 2010; Furbish et al., ~~2012~~2012b). Even in a steady flow, a sediment particle spends most of its time at rest on the bed; its journeys downstream are rare and short events (Lajeunesse et al., 2017). Overall, the combination of these stochastic events generates a downstream discharge of sediment, referred to as "bedload transport", whose intensity depends on the properties of the flow, and on the ~~grain~~ size, density, and shape of the sediment particles (Einstein, 1950; Bagnold, 1973, 1977).

Bedload transport accounts for a large part of the sediment load exported ~~out of~~from mountainous catchments (Métivier et al., 2004; Meunier et al., 2006; Liu et al., 2008). It carves the ~~channel~~channels of bedrock rivers, controls the shape and size of alluvial rivers, and generates ripples, dunes, bars and terraces (Gomez, 1991; Church, 2006; Seminara, 2010; Devauchelle et al., 2010; Aubert et al., 2016; Métivier et al., 2017; Dunne and Jerolmack, 2020; Abramian et al., 2020). In the field, geomorphologists measure bedload by collecting the moving particles in traps or baskets (Helley and Smith, 1971; Leopold and Emmett, 1976; Habersack et al., 2016). These direct measurements are laborious, and ~~sometimes risky.~~can be dangerous during flood events. These difficulties have motivated the development of alternative methods. One may, for example, estimate the intensity of bedload transport from the acoustic or seismic noise it generates (Burtin et al., 2008, 2011, 2014; Turowski and Rickenmann, 2009; Mao et al., 2016). However, the calibration of these seismic and acoustic proxies still requires direct measurements (Gimbert et al., 2014; Thorne, 2014; Burtin et al., 2016).

An alternative is to monitor the displacements of individual particles (Dietrich and Smith, 1984). These tracers~~—~~, often painted pebbles or boulders, or Radio Frequency Identification Passive Integrated Transponders (RFID PIT) inserted into the ~~boulder~~pebbles or the boulders, travel with the flow during floods (Cassel et al., 2020). Between two floods, one may ~~look~~locate for the tracers on the exposed river bed. By repeating this procedure, one gradually reveals the trajectories of the tracers. Although laborious, this method provides reliable information, without perturbing the flow. Tracer particles have been used to evaluate the storage of particles in the sediment bed (Haschenburger and Church, 1998; Bradley, 2017~~),~~) and to estimate the distance that a bedload particle travels before it settles ~~down~~downstream (Ferguson and Wathen, 1998; Martin et al., 2012). When ~~their number is large,~~the population of tracers ~~form~~is large enough, its transport forms, its transport results in a plume~~, which~~ that disperses as it travels downstream (Bradley and Tucker, 2012; Phillips and Jerolmack, 2014). ~~One may~~It is then possible to infer the mean bedload discharge from the elongation of this plume (Lajeunesse et al., 2018).

Measuring bedload transport, nonetheless, remains arduous~~,~~ and some questions are still open. On average, how often ~~can~~does a river transport its coarsest sediment? How long does a boulder remain on the river bed? ~~We propose a new approach to~~We address these questions with a new approach. Instead of tracking the particles when they travel, we monitor the evolution of their population at a fixed location. In that sense, our method can be called "Eulerian~~"~~." as opposed to Lagrangian particle tracking. Using a drone, we recorded yearly images of the bed of the Vieux Habitants river (section 2), a gravel-bed river

located in Basse-Terre Island (Guadeloupe, French West Indies). As the resolution of our images does not allow us to observe particles smaller than 0. 10 to 0.15 m, we restrict our analysis to sediment of size between 0.5 and 0.75 m. Given the resolution of our images, these boulders are indeed easier to track. However, the method we propose can be extended to smaller grains given the appropriate image resolution. Combined with high frequency measurements of the river discharge, these images allow us to (1) ~~to~~ follow the population of boulders (Terry and Goff, 2014) that make up the bed~~,~~ and (2) ~~to determine the threshold discharge above which the flow puts these boulders into motion (section 3), and (3) to estimate the residence time of boulders~~characterize the evolution of bedload transport in ~~the~~this river ~~bed~~over eight years.

2 Field site, measurement and processing

We conducted our investigation on Basse-Terre Island, a volcanic island of the Guadeloupe archipelago~~,~~ which is part of the subduction arc of the Lesser Antilles (Feuillet et al., 2002 - Fig. 1a). Basse-Terre's climate is tropical~~,~~ with daily temperatures between 24 and 28 °C, and an average rainfall rate of about 5200 mm y^{-1}. ~~Rains occur~~Rainfall occurs mainly as short and intense events. During the rainy season, which extends from June to January, storms and hurricanes are frequent~~,~~ and the rainfall rate may reach up to 590 mm day^{-1}. As a result, the discharge of rivers varies ~~abruptly,~~rapidly with frequent flash floods.

Rad et al. (2006) estimated the mechanical erosion rate of several Basse-Terre catchments based on a comparison between the chemical composition of the dissolved load~~,~~, the solid weathered load and the unweathered rocks. They found that ~~it~~the chemical erosion is about 100-120 t km^{-2} y^{-1} while the mechanical erosion varies between 800 and 4000 t km^{-2} y^{-1}, or, equivalently, 0.3 and 1.5 mm y^{-1} ~~(~~for a rock density of about 2900 kg m^{-3}~~).~~. These values are consistent with the volume of sediment mobilized by landslides during extreme climatic events (Allemand et al., 2014). ~~They place~~These estimates make Basse-Terre Island ~~amongst~~one of the fastest eroding places on Earth (Summerfield and Hulton, 1994). This observation led to the creation of the "Observatoire de l'Eau et de l'éRosion aux Antilles" (ObsERA), an observatory which monitors erosion within the French Network of Critical Zone Observatories (Gaillardet et al., 2018). Our field site is located in the Vieux-Habitants catchment which is monitored by ObsERA.

The Vieux-Habitants river (Fig. 1b) drains a 30 km^2 watershed on the leeward (West) side of the island. Most of the watershed, made of andesitic lava and pyroclastic deposits ~~aged from~~between 600 to 400 ky~~,~~ old (Samper et al., 2007), is covered with a dense rain forest ~~(Samper et al., 2007).~~. The Vieux-Habitants river flows over 19 km, from its headwater at an altitude of 1300 m, down to the Vieux-Habitants village, where it discharges into the Caribbean Sea. The channel is made of bedrock~~,~~ partly covered with a thin layer of alluvial sediment. Five kilometers from the sea, the river ~~turns~~becomes alluvial~~,~~ and its slope gradually decreases. Our ~~field site is~~study focuses on a reach of the Vieux-Habitants river located 3 km from the sea~~,~~ at an elevation 45 m a.s.l. There, the river bed is alluvial and the channel~~,~~ meanders between two steep banks about 2.5 m high. A

large ~~boulder~~ bar of pebbles and boulders, 300 meters long and 35 meters wide, lies on the inner side of the channel (Fig. 1c, d).

The *Direction de l'Environnement, de l'Aménagement et du Logement* (DEAL-Guadeloupe) operates a stream gauge~~,~~ at the Barthole station, three kilometers upstream of our field site (Fig. 1b). This station has been measuring the river discharge every ten minutes for more than 15 years~~,~~ except for ~~an interruption~~a hiatus between 2009 and 2011. As no major tributary joins the main stream between Barthole and our field site, we shall assume that the data acquired in Barthole provides a reasonable estimate of the river discharge at our site.

~~The data acquired between~~Between 2011 and 2018 ~~reveals that~~, the discharge stays below 10 m^3 s^{-1} for 91% of the time (Fig. 2a). In this low flow state, the ~~boulder~~ bar emerges and the river flows in a channel that forms between the bar and the left bank of the river (Fig. 1d). There, the water depth is about 0.3 m, but may locally exceed 0.7 m (Fig. 1c, d). Floods are characterized by a steady increase of the discharge ~~during~~for 1 to 6 hours~~,~~ followed by a recession that lasts typically 4 to 18 hours (Fig. 2b - Guérin et al., 2018). The largest flood ever recorded in Barthole occurred during hurricane Maria~~,~~ from September 18 to September 19~~,~~ 2017. The water discharge then reached more than 250 m^3 s^{-1}~~, flooding not~~ and the river flooded non only the bar but also ~~the river's~~its banks. After the hurricane, the river returned to its normal course~~,~~ along the left side of the bar.

To understand how floods affect the river's bed, we acquired aerial images of our field site with an uncrewed hexacopter Aerial Vehicle named DRELIO (~~for~~ *DRone hELIcoptère pour l'Observation de l'environnement*). This ~~device~~aircraft, specially designed for tropical conditions, is capable of flying in steep~~,~~ and densely vegetated watersheds~~, and~~. It requires only a small takeoff area (Delacourt et al., 2009~~). It~~) and carries a high resolution camera. We started working in 2011, with a Nikon D700 reflex camera, equipped with a 35 mm lens. In 2016, we replaced it with a Sony Alpha 7 reflex, still in use at present. As a result, the resolution of our images improved from 0.04 ~~meters~~m/pixel in 2011 to 0.02 meters/pixel starting from 2016.

From 2011 to 2018, we performed 8 field campaigns following the same procedure. We flew DRELIO at an elevation of 80 m above the river bed~~,~~ and used the on-board camera to acquire a series of images that covered the entire ~~boulder~~ bar with an 30% overlap between two neighboring images. Using the MicMac Photogrammetric suite (Rupnik et al., 2017), we ~~computed~~compute for each campaign a Digital Surface Model (DSM) and an orthoimage of the bar. ~~An orthoimage is an image from which the distortion due to relief has been suppressed. Two georeferenced~~The orthoimages ~~of the same surface can be superimposed. Each orthoimage is~~are georeferenced using fixed ground control points~~,~~ whose coordinates are measured by Differential Global Navigation Positioning System. The resulting resolution of the orthoimages ranges from 0.04 ~~m~~to 0.02 m depending on the acquisition year.

To monitor the evolution of the bar, we superimpose the georeferenced orthoimages using a GIS software (QGIS in our case). However, the georeferencing is not perfect~~and the series~~. The quality of ~~diachronic orthoimages do not exactly overlap. We selected~~the superimposition degrades with the distance from the ground control points (e.g. Jaud et al., 2019a). To reduce this

4

distortion, we use the 2012 orthoimage as the "base image" and warp the others on that base using a minimum of 15 control points (Jaud et al., 2019b).

We then trace the contour of the boulders visible on each orthoimage using a raster graphic editor. The diameter of the smallest visible grains is 5 pixels (0.1 to 0.15 m). On the bar, however, most boulders have a diameter larger than 0.2 m, and some are larger than 1 m (Terry and Goff, 2014). In practice, we restrict our analysis to boulders with a diameter larger than 0.5 m as they are clearly distinguishable on the images. Using QGIS, we then vectorize the contours of the boulders and calculate their exposed area, A, from which we deduce the boulder equivalent diameter defined as the diameter D of a disk with the same surface area, $D = 2\sqrt{A/\pi}$. We estimate that the uncertainty on the area, A, is between 15 and 20 % for the smaller diameters. With this method, we obtain 8 diachronic superimposable orthoimages and 8 vector files of the boulders shapes, position and equivalent diameter.

We visually compared two orthoimages of the bar (fig. 3) from 2012 and 2013 and found that several boulders have been removed or deposited in between. Several boulders (yellow contours in Fig. 3), lying on the bar in 2012, are not visible in 2013: they were entrained downstream by the river at some time between two acquisition campaigns. In 2013, we also find several boulders that were absent in 2012 (red contours in Fig. 3): these boulders have been deposited on the bar sometime between the two image campaigns. Finally, the rest of the boulders (blue contours in Fig. 3) remained in place. The comparison between two consecutive GIS thus allows us to identify the fate of each boulder. Based on this method, we attribute a label to each boulder of each image which specifies whether the boulder was already in place during the previous campaign, or if it was deposited recently. Some cases turn out to be ambiguous: a few boulders disappeared and then reappeared on more recent images, as floods covered them with sediment, before exposing them again. Those ambiguous cases were duly labelled and the corresponding boulders were considered immobile. Following this procedure, we produce a dataset that contains the position, size and transport history (deposited, entrained, or immobile) of all the boulders larger than 0.5 m. In short, we treat the boulders as tracers to characterize their transport of boulders in the Vieux-Habitants river.

3 Results

3.1 Structure of the bar: mobile and consolidated layers ~~—~~

~~Our~~A visual inspection of our data show that entrained and deposited boulders are uniformly distributed over the whole bar. There is no particular place from which boulders ~~were~~are preferentially exported, nor onto which they ~~were~~are preferentially deposited. This suggests that, during floods, bedload transport is uniform over the bar.

Our dataset also reveals the existence of two ~~families~~populations of immobile boulders. The first ~~one~~ corresponds to boulders that were deposited on the bar during the course of our survey~~,~~ and remained immobile for several years~~,~~ until the river entrained them again. The second ~~one~~ corresponds to boulders that ~~remained immobile during the whole survey. The latter~~ are partially buried in a matrix of ~~smaller sediment~~fine sediments and ~~appear to belong to a stable underlying base layer, that spans over~~remained immobile for the whole duration of the ~~entire bar~~survey. These observations are consistent with the concept of active layer (e.g. Church and Haschenburger, 2006). We therefore interpret them as ~~the result of the existence of two~~an indication that there are two distinct layers of boulders: (i) an active surface layer of mobile boulders, and (ii) an underlying basal layer of static ones. ~~Interestingly, laboratory~~Laboratory experiments report a similar ~~division~~partition between an active layer of mobile grains, that regularly settle on the bed until the flow eventually dislodges them and set them back ~~in~~into motion, and a layer of static grains (Charru et al., 2004, Lajeunesse et al., 2010). In the following, we ~~focus on the properties of~~investigate the layer of mobile boulders.

3.2 ~~Granulometric~~ Grain-size distribution

We ~~start our analysis by focusing~~first focus on the motion of boulders of size between 0.5 and 2 ~~meters~~m. To characterize their distribution, we divide ~~this interval~~ the population of boulders into six 0.25 m-wide bins~~, and distribute the boulders in each one, according to their equivalent diameter~~. We then compute the dimensionless surface density of each class i, defined as the number of grains per unit surface, normalized by the area of a grain:

$$\tilde{\sigma}_i = \frac{\cancel{N_i \times \pi D_i^2}}{\cancel{S}} \frac{N_i \pi D_i^2}{S_b} .$$ (1)

where N_i is the number of boulders in class i, D_i is their equivalent diameter, and ~~S~~S_b=2000 m^2 is the area of the bar. The dimensionless surface density σ_i can also be interpreted as the ~~proportion~~fraction of the bar area occupied by the boulders of class i.

The number of boulders in each class and the corresponding surface density vary from year to year. To account for these variations, we compute these two quantities for each field campaign~~, and represent the results in the form of a box plot (Fig.~~ (Fig. 4a). We find that the surface density of each class varies by less than 27% around its median ~~value~~. The size distribution of the boulders thus does not change significantly ~~with~~over time, but appears to be roughly at equilibrium. This equilibrium is not static, but dynamic. Indeed, distinguishing the boulders freshly deposited (Fig. 4a, green boxes) from those that were

already in place during the preceding campaign (Fig. 4a, yellow boxes) shows that about half of the population of boulders is renewed each year ~~(Fig. 4a).~~. In short, the number of boulders entrained by floods balances, on average, the number of fresh boulders deposited on the bar~~,~~ thus ~~maintaining constant~~ keeping their surface density constant (Fig. 4b).

Finally, our analysis shows that the surface density rapidly decreases with grain size (Fig. 4a). With a surface density $\sigma = 0.23$ boulders m^{-2}, or equivalently, a total number of about 350 boulders over the 2000 m^2 of the bar, boulders of size 0.5 to 0.75 m dominate the bar, at least in the range of diameters accessible to our ~~measurement~~measurements. The transport rate of these boulders is also sufficiently high to allow for significant statistics. In the following, we shall therefore focus on the transport of boulders of size 0.5 to 0.75 m. ~~Before we do so, however, we first need to evaluate the threshold discharge above which these boulders are set in motion. This is the topic of the next section.~~

3.3 Threshold for the initiation of transport

Based on our dataset, we can identify the largest boulders deposited on, or entrained from, the bar between two consecutive campaigns~~. Plotting their diameter as a function~~ for each of the ~~maximum water discharge between two~~8 campaigns~~,~~ we ~~performed. We~~ find that the maximum size of ~~these~~both entrained and deposited boulders increases with the maximum discharge (Fig. 5). Assuming that the largest boulders are transported when the discharge is at its highest, the resulting curve provides a reasonable estimate of the threshold discharge beyond which grains of a given size are entrained by the flow. ~~For lack of sufficient data, however, we cannot~~ This method allows us to estimate the threshold discharge of ~~boulders smaller~~ particles larger than 0.~~5~~75 m. Below this size, particles are entrained during floods of lesser amplitude that occur several times a year, and we cannot measure their threshold discharge based on our yearly observations. Instead, we shall now try to ~~evaluate~~calculate it~~,~~ by extrapolating ~~from~~ our observations towards smaller grain sizes.

In practice, the threshold discharge corresponds to the discharge for which the shear stress exerted by the river on its bed exceeds a critical value (Shields, 1936). The instantaneous turbulent stress exerted on the river bed is, however, highly variable in space and in time: it depends on the flow, ~~on~~ the shape of the channel, ~~on~~ the river slope, ~~on~~and the bed roughness~~, and its~~. Its measurement in the field is challenging (Henderson~~,~~ 1963~~;~~; Parker~~,~~ 1978~~;~~; Chauvet et al., 2014~~;~~; Métivier et al., 2017~~;~~; Nezu and Nakagawa, 1993). Here, to simplify the problem, we assimilate the river geometry to that of a ~~rectangular channel~~rectangle of width W, depth H, and slope S. Based on the Darcy-Weisbach equation, we then derive the threshold discharge required to transport a boulder (see appendix for a full derivation):

$$Q_c = W \frac{D^{3/2}}{S} \left(\theta_c \frac{\Delta\rho}{\rho} \right)^{3/2} \left(\frac{g}{C_f} \right)^{1/2} \tag{2}$$

where $\Delta\rho$ ~~$= \rho_s - \rho$~~ is the difference between the rock density ~~of rock~~(ρ_s) and ~~that of~~ water~~,~~ density (ρ), C_f is the Darcy-Weisbach friction parameter, g is the acceleration of gravity, and θ_c is the threshold Shields parameter (Shields, 1936). Our model is crude and some of the parameters in equation (2) are difficult to estimate. Based on direct field measurements, we estimate the river width to be W=30 m. Using the DEM, we calculate ~~its~~an average slope ~~and find it to be~~of about S ~~=~~ =0.03. For the

friction coefficient, we use the value $C_f = 0.1$, typical of mountain streams (Limerinos, 1970). A fit of equation (2) to our data

215 reasonably accounts for our observations (Fig. 5~~),~~) and yields a threshold Shields stress Θ_c=0.032~~,~~ which falls in ~~a realistic~~the range reported by previous compilations of critical Shields stress measurements from field settings (Buffington and Montgomery, 1997; Lamb et al., 2008). Combining this value with equation (2), we find that the threshold discharge of the boulders of size 0.5 to 0.75 m is 45 +/- 20 m^3s^{-1}, where the uncertainty range derives from the bounds of the size class. In the next section, we use this central value of 45 m^3s^{-1} to estimate the time during which the river effectively transports these

220 boulders.

~~Encouraged by this result, we use equation (2) to calculate the threshold discharge of the boulders of size 0.5 to 0.75 m. We find a threshold discharge between 24 and 69 m^3s^{-1}, with a value of 45 m^3s^{-1} for the intermediate Shields number of 0.032. In the next section, we use this value to estimate the time during which the river effectively transports these boulders.~~

3.4 Effective transport time

225 ~~Boulders~~In the previous section, we calculated that boulders of size 0.5 to 0.~~75m~~75 m move only when the river discharge exceeds the threshold value of 45 ~~m^3s^{-1} calculated in the previous section. Their~~+/- 20 m^3s^{-1}. The corresponding effective transport time ~~is therefore~~, i.e. the ~~cumulated~~cumulative time that the river spends above this threshold ~~(Fig. 6). We find that it,~~ amounts to a total of 85 ~~hours~~h for the period that extends from January 2011 to May 2018~~.~~ (Fig. 6). The time fraction during which the river is above the entrainment threshold is thus $I = 0.12\%$. This means that, on average, boulders ~~can move~~are

230 transported during about 10 hours each year.

The effective transport time depends on the occurrence of floods~~,~~ and therefore~~,~~ on the distribution of rainfalls. As the latter varies from year to year, so does the effective transport time (Fig. 6~~): the~~). The river spent less than 5 hours above 45 m^3s^{-1} between 2014 and 2016 (an unusually dry period). Conversely, it spent 32 hours above 45 m^3s^{-1} between 2017 and 2018, a period that includes hurricane Maria. Even ~~during those years~~then, the annual effective transport time did not exceed 0.36%

235 of the year~~that is about 30 hours.~~. On a tropical volcanic island like Guadeloupe, ~~the~~ boulders move only during very short periods of time~~,~~ whose ~~cumulated~~cumulative duration depends on the frequency and the intensity of the storms.

3.5 Evolution of the population of boulders

~~So far~~In the previous section, we ~~have focused on~~calculated the threshold of transport and the effective transport time of boulders. ~~We~~ Based on these results, we now use our ~~data~~dataset to ~~document~~measure the evolution of ~~their population. As~~

240 ~~in~~the populations of boulders as function of the effective transport time. As in the previous sections, we restrict our analysis to boulders of size 0.5 to 0.75m. ~~We start by identifying~~Using our GIS, we identify all the boulders ~~lying~~of this size present on the bar in 2011. ~~Using our dataset, we~~We find that 619 boulders make up the 2011 boulder population. We then monitor the evolution of this population~~.~~, year after year, until 2018. We find that ~~its number~~the 2011 population decreases

monotonously with the effective transport time, as boulders are progressively entrained by floods, and replaced with new ones (Fig. 7), an observation similar to those of Wilcock and McArdell (1997) and Harchenbucher and Wilcock (2003).

Repeating the same procedure with the boulders lying on the bar in 2012, and the following years until 2017, To check the robustness of this observation, we apply the same procedure to a new population of boulder that is the 2012 population composed of the boulders deposited on the bar between the campaigns of 2011 and 2012. We find that it follows the same trend as the 2011 population (Fig. 7). Repeating the same procedure with the populations of boulders deposited in 2013, 2014, 2015, 2016, and 2017, we end up monitoring a total of seven populations of boulders. To compare their evolution, we normalize the number of boulders in each population with its initial value, and plot the result as function of the effective transport time (Fig. 7). We find that all data points gather around the same trend: the number of boulders decreases rapidly at first. With time, however, the rate gradually slows down.

As the surface density of boulders is small ($\sigma = 0.23$ boulder m^{-2} - see section 3.2), we expect little interaction between them during transport. Following Einstein (1937) and Charru et al. (2004), we thus assume that the number of boulders that leave the bar is proportional to the number of boulders available on its surface, that is:

$$\frac{dN}{dt} = -\frac{N}{\tau} \qquad (3)$$

where t is the effective transport time, N is the number of boulders on the bar surface at time t, and τ is a characteristic entrainment time. The solution of Eq. (3), $N = N_0\,e^{-t/\tau}$, is a decaying exponential, of characteristic time τ, where N_0 is the initial number of boulders. Fitting this exponential solution to our data yields a good representation of the evolution of N ($R^2 = 0.84$). We find) with a characteristic time $\tau = 17$ hours (Fig. 7).

The model proposed here is simplistic. It does not take into account the variations of discharge during a flood, and relies on a crude description of the threshold of transport. Yet, the exponential decrease of an initial population of boulders is consistent with the data plotted on figure 7, and we. We therefore expect that the value of the characteristic time τ is a reasonable estimate of the residence time of boulders on the bar, expressed in terms of the effective sediment transport time. This residence time is short. Expressed in terms of half-life, it takes an effective transport time of log2 $\tau = 12$ hours to entrain half of the boulders initially present on the bar, and to replace them with new ones. . As the total boulder population on the bar is at steady state (Fig. 4b), each boulder entrained out of the bar is, on average, replaced by a new one.

4. Discussion - Conclusion

To the best of our knowledge, we present here the first attempt at characterizing bedload transport based on yearly UAV image acquisition. As the resolution of our images does not allow us to observe particles smaller than 0. 10 to 0.15 m, so we restrict our analysis to boulders of size between 0.5 and 0.75 m, which are easier to track. In principle, however, the method we propose can be extended to smaller grains, given the appropriate image resolution.

Despite — or, maybe, owing to — its simplicity, the method proves robust: the comparison of images taken one year apart ~~allowed~~allows us to monitor the evolution of the population of boulders at the surface of the Vieux-Habitants river. Using high frequency measurements of the river discharge, we determine the threshold discharge necessary to set these boulders in motion~~,~~ and estimate the time during which the flow is strong enough to transport them. ~~The model of threshold we use, despite its simplicity, reproduces well our observations for a realistic range of parameters.~~

In the Vieux-Habitants river, this effective transport time amounts to an average of 10.5 hours per year ~~on average~~, that is about I=0.12% of the total time. The transport of boulders is therefore a rare event controlled by the occurrence of floods, which, in its turn, depends on the ~~distribution of rainfalls. A change of this distribution is likely to impact the quantity of sediment transported by the river.~~ rainfall regime. This result is consistent with previous observations reported for different contexts (e.g. Lague et al., 2005; Phillips and Jerolmack, 2016; Pfeiffer and Finnegan, 2018). Since climate models predict a change of the rainfall regime in the Antilles, with an increase of the frequency of extreme events (e.g. Jury and Bernard, 2020), we expect a significant increase in the sediment load delivered by Caribbean rivers to the ocean.

Einstein (1937) ~~was the~~ first ~~to propose~~proposed that the entrainment of bedload particles is an inherently ~~a~~ random process. This hypothesis is at the core of ~~the entrainment-deposition model~~ most models of bedload transport (Charru et al., 2004; ~~Lajeunesse et al.,~~Ancey, 2010; Lajeunesse et al., 2010, 2018~~). When~~; Furbish et al, 2012a, 2012b). All these models assume that, for a given shear stress, the probability to dislodge a grain from the bed is proportional to the number of grains at repose on the bed. Laboratory experiments have long confirmed this hypothesis in flumes, where a steady flow shears a flat bed of homogenous sediment (Lajeunesse, 2010; Charru et al., 2004; Ancey, 2010; Lajeunesse et al., 2010, 2018; Furbish et al., 2012a, 2012b). The results reported in this article suggest that this same assumption holds in also in natural rivers as well, even though their bed, made of very heterogeneous grains, is subject to large flow variations. Indeed, when expressed in terms of ~~the~~ effective transport time, ~~our data are consistent with this assumption:~~ the population of boulders on the bed of the Vieux-Habitants river decreases exponentially~~,~~ as expected for a ~~random~~ Poisson process.

The characteristic time of this exponential decay — in fact, the typical residence time of the boulders on the ~~bed~~bar — is short: $\tau = 17$ hours of effective transport time. The half-life of a boulder on the bar, that is the time after which a boulder population is halved, is around 10.5 h. The surface layer of the bar is thus entirely renewed every 4 to 5 years. This suggests that the residence times of a boulder in a river is likely much shorter than the time it spends trapped on hillslopes, a hypothesis consistent with assumptions commonly used in cosmogenic dating (e.g. Carretier et al., 2020).

~~We suggest a method to estimate the sedimentary discharge associated to boulder transport, based on the exponential decay of a population of well-identified boulders. During a flood, entrained boulders will travel over a distance L_f that depends on the duration and on the intensity of the flood. The discharge of boulders across a given section of the river is the number of grains entrained per unit time, from a bed area of size WL_f. The boulder discharge is therefore the total number of boulders at rest on~~

10

this surface, $\sigma W L_f$, divided by the residence time, τ, where σ is the surface density of boulders (Einstein, 1937). The instantaneous volumetric discharge is then the number of grains entrained by unit time, times the average volume of grains. To convert this value into an annual sediment flux, we multiply it by the proportion of time, I, during which the river is above the entrainment threshold. L_f is the most difficult parameter to estimate. It can be approached by using a tranport law (Lajeunesse et al., 2010) or measured in the field using RFID tracers as proposed by Phillips and Jerolmack (2014). On a yearly timescale, the discharge of boulders scales like $Q \sim \sigma$ W L_f/τ, where τ is the residence time of the boulders on the bar, σ is their number per unit area of the bed, W is the river width and L_f is the average distance traveled by a boulder during a year (Einstein, 1937). At present, we cannot use this formula to calculate the discharge of boulders in the Vieux-Habitants river, for lack of measurement of the traveled distance L_f. However, this distance has been measured in other contexts with tracer pebbles equipped with Radio Frequency Identification (RFID) PIT tags (e.g., Bradley and Tucker, 2012, Phillips and Jerolmack, 2014, Papangelakis et al., 2019). The combination of this RFID technique with the UAV method that we report here should allow us to estimate both the residence time and the distance traveled by bedload particles, and therefore the bedload discharge (Papangelakis et al., 2022).

Obviously, the approach that we propose here has many limitations. The major one is that the intermittent burial of boulders, that may occur at high sediment discharge, is not accounted for. In the Vieux-Habitants river, such burial is unlikely because the sedimentary active layer has a thickness of about one boulder diameter. In other settings, however intermittent burial might play a significant role (e.g. Yager et al., 2012). The use of boulders marked with RFID PIT tags might help to counter this problem.

Code/Data availability

Discharge data used for figures 2 and 6 are available on http://www.hydro.eaufrance.fr/. UAV Images and dataset are available on Harvard Dataverse https://dataverse.harvard.edu/dataset.xhtml?persistentId=doi:10.7910/DVN/QRHM8E

Author contributions

PA designed and performed the field measurements, and processed the resulting data. All authors developed the overall ideas and were responsible for critical contributions, passing the final manuscript and editing text and figures.

Competing interests.

The authors declare no competing interests.

Appendix A - Threshold discharge

Here, we estimate the threshold discharge above which the river can transport its sediment. To do so, we assimilate the channel to a rectangle of width W, depth H, and slope S. The Darcy-Weisbach equation then relates the average flow velocity V to the shear stress τ exerted on the river bed (Limerinos, 1970):

$$\tau = C_f \rho V^2 \tag{A1}$$

where ρ is the density of water and C_f is the Darcy-Weisbach friction coefficient. In steady state, the momentum balance requires that:

$$\tau = \rho g S H. \tag{A2}$$

At the onset of sediment motion, the Shield number, Θ, defined as the ratio between the driving force acting on the grains and the weight of a grain, must equal a threshold value Θ_c:

$$\Theta = \frac{\tau}{\Delta \rho g D} \quad\quad = \Theta_c, \tag{A3}$$

where Δρ is the difference between the density of a grain and that of water, g, is the acceleration of gravity, and D is the grain size. Combining (A2) with (A3) yields the expression of the flow depth H at the threshold of entrainment:

$$H = \Theta_c \frac{\Delta \rho}{\rho} \frac{D}{S}. \tag{A4}$$

Similarly, combining (A1) with (A2) and (A3) yields the average flow velocity at the threshold of entrainment:

$$V = \left(\Theta_c \frac{\Delta \rho}{\rho} \frac{gD}{C_f} \right)^{1/2}. \tag{A5}$$

Injecting the velocity and the flow depth into the expression of the water discharge, $Q = WHV$, we find the threshold discharge above which the river can transport a boulder of diameter D:

$$Q_c = W \frac{D^{3/2}}{S} \left(\Theta_c \frac{\Delta \rho}{\rho} \right)^{3/2} \left(\frac{g}{C_f} \right)^{1/2} \tag{A7}$$

This expression, of course, is only a crude estimate, if only because the river is not a straight rectangular channel. Nonetheless, it provides a decent approximation of the flow conditions that are necessary to initiate the transport of a given class of boulders (Figure 5).

References

360   Abramian, A., Devauchelle, O., and Lajeunesse, E.: Laboratory rivers adjust their shape to sediment transport, Physical Review E, 102, 053101, doi: 10.1103/PhysRevE.102.053101, 2020.

Allemand, P., Delacourt, C., Lajeunesse, E., Devauchel, O., and Beauducel, F.: Erosive effects of the storm Helena (1963) on Basse Terre Island (Guadeloupe — Lesser Antilles Arc), Geomorphology, doi: 10.1016/j.geomorph.2013.09.020, 2014.

Ancey, C.: Stochastic modeling in sediment dynamics: Exner equation for planar bed incipient bed load transport conditions. Journal of Geophysical Research: Earth Surface, 115, 10.1029/2009JF001260, 2010.

365

Ancey, C., Davison, A., Bohm, T., Jodeau, M., and Frey, P.: Entrainment and motion of coarse particles in a shallow water stream down a steep slope, J. Fluid Mech., 595, 83–114, doi: 10.1017/S0022112007008 774, 2008.

Aubert, G., Langlois, V.J., Allemand, P.: Bedrock incision by bedload: insights from direct numerical simulations, Earth Surf. Dynam., 4, 327–342, doi: 10.5194/esurf-4-327-2016, 2016.

370   Bagnold, R.: The nature of saltation and of Bedload transport in water, Proc. R. Soc. Lond., A 332, 473–504, 1973.

Bagnold, R.: Bedload transport by natural rivers, Water Resources Research, 13, 303–312, 1977.

Bradley, D. N.: Direct Observation of Heavy-Tailed Storage Times of Bedload Tracer Particles Causing Anomalous Superdiffusion, Geophysical Research Letters, 44, doi: 10.1002/2017GL075045, 2017.

Bradley, D. N. and Tucker, G. E.: Measuring gravel transport and dispersion in a mountain river using passive radio tracers, 375   Earth Surface Processes and Landforms, 37, 1034–1045, doi: 10.1002/esp.3223, 2012.

Buffington, J., and Montgomery, D.: A systematic analysis of eight decades of incipient motion studies, with special reference to gravelbedded rivers, Water Resour. Res., 33, 1993–2029, doi: 10.1029/97WR03138, 1997.

Burtin, A., Bollinger, L., Vergne, J., Cattin, R., and Nábelek, J.: Spectral analysis of seismic noise induced by rivers: A new tool to monitor spatiotemporal changes in stream hydrodynamics, Journal of Geophysical Research: Solid Earth, 113, doi: 380   10.1029/2007JB005034, 2008.

Burtin, A., Cattin, R., Bollinger, L., Vergne, J., Steer, P., Robert, A., Findling, N., and Tiberi, C.: Towards the hydrologic and bedload monitoring from high-frequency seismic noise in a braided river: The "torrent de St Pierre", French Alps, Journal of hydrology, 408, 43–53, doi: 10.1016/j.jhydrol.2011.07.014, 2011.

385   Burtin, A., Hovius, N., McArdell, B., Turowski, J., and Vergne, J.: Seismic constraints on dynamic links between geomorphic processes and routing of sediment in a steep mountain catchment, Earth Surf. Dynam., 2, 21–33, doi: 10.5194/esurf-2-21-2014, 2014, 2014.

Burtin, A., Hovius, N., and Turowski, J. M.: Seismic monitoring of torrential and fluvial processes, Earth Surf. Dynam., 4, 285–307, doi: 10.5194/esurf-4-285-2016, 2016.

390   Carretier, S., Guerit, L., Harries, R., Regard, V., Maffre, P., and Bonnet, S.: The distribution of sediment residence times at the foot of mountains and its implications for proxies recorded in sedimentary basins, Earth Planet. Sc. Lett., 546, 116448, doi: 10.1016/j.epsl.2020.116448, 2020.

Cassel, M., Piegay, H., Fantino, G., Lejot, J., Bultingaire, L., Michel, K. and Perret, F.: Comparison of ground-based and UAV a-UHF artificial tracer mobility monitoring methods on a braided river, Earth Surf. Process. Landforms, 5, 1123-1140, doi: 10.1002/esp.4777, 2020.

395   Charru, F., Mouilleron, H., and Eiff, O.: Erosion and deposition of particles on a bed shared by a viscous flow, Journal of Fluid Mech., 519, 55–80, doi:10.1017/S0022112004001028, 2004.

Chauvet, H., Devauchelle, O., Métivier, F., Lajeunesse, E., and Limare, A.: Recirculation cells in a wide channel, Phys. Fluids, 26, 016604, 1–10, doi: 10.1063/1.4862442 2014.

Church, M.: Bed material transport and the morphology of alluvial river channels, Annu. Rev. Earth Planet. Sci., 34, 325–354, 400   doi: 10.1146/annurev.earth.33.092203.122721, 2006.

Church, M., and Haschenburger, J.K.: What is the "Active Layer"? Water Resour. Res. 2017, 53, 5–10, doi: 10.1002/2016WR019675, 2017.

Delacourt, C., Allemand, P., Jaud, M., Grandjean, P., Deschamps, A., Ammann, J., Cuq, V., and Suanez, S.: DRELIO: An unmanned helicopter for imaging coastal areas, SI 56, Proceedings of the 10th International Coastal Symposium), 1489-1493, 405   Lisbon, Portugal, 2009.

Devauchelle, O., Malverti, L., Lajeunesse, E., Lagrée, P., Josserand, C., and Thu-Lam, K.: Stability of bedforms in laminar flows with free surface: from bars to ripples, Journal of Fluid Mechanics, 642, 329–348, doi: 10.1017/S0022112009991790, 2010.

Dietrich,W. and Smith, J.: Bedload Transport in a River Meander, Water Resources Research, 20, doi: 410   10.1029/WR020i010p01355, 1984.

Dunne, K. B. and Jerolmack, D. J.: What sets river width? Science advances, 6, doi: 10.1126/sciadv.abc1505, 2020.

Einstein, H.: The bed-load function for sediment transportation in open channel flows, US Department of Agriculture. Soil Conservation Service, 1950.

Einstein, H. A.: Bedload transport as a probability problem, in: Sedimentation: 746 Symposium to Honor Professor H.A. Einstein, 1972. translation from 747 German of H.A. Einstein doctoral thesis. Originally presented to Federal Institute of Technology, Zurich, Switzerland, 1937, pp. C1 – C105, 1937.

Ferguson, R. and Wathen, S.: Tracer-pebble movement along a concave river profile: Virtual velocity in relation to grain size and shear stress, Water Resources Research, 34, 2031–2038, doi: 10.1029/98WR01283, 1998.

Feuillet, N., Manighetti, I., and Tapponnier, P.: Arc parallel extension and localization of volcanic complexes in Guadeloupe, Lesser Antilles. J. Geophys. Res., 107, 1-29, doi: 10.1029/2001JB000308, 2002.

Furbish, D., Roseberry, J., and Schmeeckle, M.: A probabilistic description of the bedload sediment flux: 3. The particle velocity distribution and the diffusive flux, Journal of Geophysical Research, 117, F03 033, doi: 10.1029/2012JF002356, 20122012a.

Furbish, D. J., Haff, P.K., Roseberry, J.C., and M. W. Schmeeckle, M.W.: A probabilistic description of the bed load sediment flux: 1. Theory, J. Geophys. Res., 117, F03031, doi: 10.1029/2012JF002352, 2012b.

Gaillardet, J., I. Braud, F. Hankard, S. Anquetin, O. Bour, N. Dorfliger, et al.: OZCAR: The French network of critical zone observatories. Vadose Zone J. 17:180067, doi: 10.2136/vzj2018.04.0067, 2018.

Gimbert, F., Tsai, V. C., and Lamb, M. P.: A physical model for seismic noise generation by turbulent flow in rivers, J. Geophys. Res. Earth Surf., 119, 2209–2238, doi: 10.1002/2014JF003201, 2014.

Gomez, B.: Bedload transport, Earth-Science Reviews, 31, 89–132, doi: 10.1016/0012-8252(91)90017-A, 1991.

Guerin, A., Devauchelle, O., Robert, V., Kitou, T., Dessert, C., Quiquerez, A., et al.: Stream-discharge surges generated by groundwater flow. Geophysical Research Letters, 46, 7447–7455. doi:10.1029/2019GL082291, 2019.

Habersack, H., Kreisler A., Rindler R., Aigner J., Seitz, H., Liedermann, M., Laronne, J.B.: Integrated automatic and continuous bedload monitoring in gravel bed rivers, Geomorphology, doi: 10.1016/j.geomorph.2016.10.020, 2016.

435   Haschenburger, J.K. and Church, M.: Bed material transport estimated from the virtual velocity of sediment. Earth Surf. Process. Landforms, 23: 791-808. ~~doi: 10.1002/(SICI)1096-9837(199809)23:9<791::AID-ESP888>3.0.CO;2-X~~doi: 10.1002/(SICI)1096-9837(199809)23:9<791::AID-ESP888>3.0.CO;2-X, 1998.

Haschenburger, J. K. and Wilcock, P.R.: Partial transport in a natural gravel bed channel. Water Resources Research, 39, 1, 1020, doi: 10.1029/2002WR001532, 2003.

440   Helley, E.J. and Smith, W.: Development and calibration of a pressure-difference bedload sampler, Geological Survey Open-File Report, December 3, 1971., 1971.

Henderson, F. M.: Stability of alluvial channels, T. Am. Soc. Civ.Eng., 128, 657–686, 1963.

Houssais, M. and Lajeunesse, E.: Bedload transport of a bimodal sediment bed, J. Geophys. Res., 117, F04015, doi: 10.1029/2012JF002490, 2012.

445   Jaud, M., Passot, S., Allemand, P., Le Dantec, N., Grandjean, P., et al.: Suggestions to Limit Geometric Distortions in the Reconstruction of Linear Coastal Landforms by SfM Photogrammetry with PhotoScan and MicMac for UAV Surveys with Restricted GCPs Pattern. Drones, MDPI, 3 (2), doi: 10.3390/drones3010002, 2019a.

Jaud, M., Delacourt, C., Le Dantec, N., Allemand, P., Ammann, J., et al.: Diachronic UAV Photogrammetry of a Sandy Beach in Brittany (France) for a Long-Term Coastal Observatory. ISPRS International Journal of Geo-Information, MDPI, 2019b, 8

450   (6), pp.267, doi: 10.3390/ijgi8060267, 2019b.

Jury, M.R. and Bernard, D.: Climate trends in the East Antilles Islands. International Journal of Climatology, 40, 36–51, doi: 10.1002/joc.6191, 2019.

Lague, D., Hovius, N., and P. Davy, P.: Discharge, discharge variability, and the bedrock channel profile, J. Geophys. Res.,110, F04006, 2005, doi: 10.1029/2004JF000259, 2005.

455   Lajeunesse, E., Malverti, L., and Charru, F.: Bedload transport in turbulent flow at the grain scale: experiments and modeling, J. Geophys. Res, 115, F04 001, doi: 10.1029/2009JF001 628, 2010.

Lajeunesse, E., Devauchelle, O., Lachaussée, F., and Claudin, P.: Bedload transport in laboratory rivers: the erosion-deposition model, in: Gravel-bed Rivers: Gravel Bed Rivers and Disasters, Wiley-Blackwell, Oxford, UK, 415–438, doi: 10.1002/9781118971437.ch15, 2017.

460   Lajeunesse, E., Devauchelle, O., and James, F.: Advection and dispersion of bed load tracers, Earth Surf. Dynam., 6, 389–399, doi: 10.5194/esurf-6-389-2018, 2018.

Lamb, M.P., Dietrich, W.E., and Venditti, J.G.: Is the critical Shields stress for incipient sediment motion dependent on channel-bed slope? J. Geophys. Res., 113, F02008, doi:10.1029/2007JF000831, 2008.

Leopold, L. B. and Emmett, W. W.: Bedload measurements, East 85 Fork River, Wyoming, Proceedings of the National
465   Academy of Sciences, 73, 1000–1004, 1976.

Limerinos, J.T.: Determination of the Manning coefficient from measured bed roughness in natural channels. United States, Geological Survey, Water-Supply Paper 1898-B, 1970.

Liu, Y., Metivier, F., Lajeunesse, E., Lancien, P., Narteau, C., and Meunier, P.: Measuring bedload in gravel bed mountain rivers: Averaging methods and sampling strategies, Geodin. Acta, 21, 81–92, doi: 10.3166/ga.21.81-92, 2008.

470   Mao, L., Carrillo R, Escauriaza C, Iroume A.: Flume and field-based calibration of surrogate sensors for monitoring bedload transport. Geomorphology, 253, 10–21. doi: 10.1016/j.geomorph.2015.10.002, 2016.

Martin, R. L., Jerolmack, D. J., and Schumer, R.: The physical basis for anomalous diffusion in bedload transport, Journal of Geophysical Research, 117, F01 018, doi: 10.1029/2011JF002075, 2012.

Métivier, F., Meunier, P., Moreira, M., Crave, A., Chaduteau, C., Ye,B., and Liu, G.: Transport dynamics and morphology of
475   a high mountain stream during the peak flow season: The ürümqi River (Chinese Tianshan), in River Flow 2004: Proceedings of the Second International Conference on Fluvial Hydraulics, edited by M. Greco et al., pp. 761– 777, Taylor and Francis, Philadelphia, Pa, 2004.

Métivier, F., Lajeunesse, E., and Devauchelle, O.: Laboratory rivers: Lacey's law, threshold theory, and channel stability, Earth Surf. Dynam., 5, 187–198, doi: 10.5194/esurf-5-187-2017, 2017.

480   Meunier, P., Metivier, F., Lajeunesse, E., Meriaux, A.S., and Faure, J.: Flow pattern and sediment transport in a braided river: The "torrent de St Pierre" (French Alps), J. Hydrol., 330, 496–505, doi: 10.1016/j.jhydrol.2006.04.009, 2006.

Nezu, I and Nakagawa, H.: Turbulence in Open Channel Flows. IAHR Monograph, A. A. Balkema, Rotterdam, 1993.

Papangelakis, E., MacVicar, B., Ashmore, P.: Bedload sediment transport regimes of semi-alluvial rivers conditioned by urbanization and stormwater management. Water Resources Research 55, 10565–10587. doi: 10.1029/2019WR025126, 2019.

Papangelakis, E., MacVicar, B. J., Montakhab, A. F., and Ashmore, P.: Flow strength and bedload sediment travel distance in gravel bed rivers. Water Resources Research, 58, e2022WR032296, doi: 10.1029/2022WR032296, 2022.

Parker, G.: Self-formed straight rivers with equilibrium banks and mobile bed. Part 1. The sand-silt river, J. Fluid Mech., 89, 109–125, 1978.

Pfeiffer, A. M., & Finnegan, N. J.: Regional variation in gravel riverbed mobility, controlled by hydrologic regime and sediment supply. Geophysical Research Letters, 45, 3097–3106; 2018, doi: 10.1002/2017GL076747, 2018

Phillips, C. B. and Jerolmack, D. J.: Dynamics and mechanics of bed-load tracer particles, Earth Surf. Dynam., 2, 513–530, doi: 10.5194/esurf-2-513-2014, 2014.

Phillips, C. B. and Jerolmack, D. J.: Self-organization of river channels, as a critical filter on climate signals, Science, 352, 694–697, doi: 10.1126/science.aad3348, 2016.

Phillips, C., Hill, K. M., Paola, C., Singer, M., and Jerolmack, D.: Effect of flood hydrograph duration, magnitude, and shape on bed load transport dynamics, Geophys. Res. Lett., 45, 8264–8271, doi: 10.1029/2018GL078976, 2018.

Rad, S., Louvat, P., Gorge, C., Gaillardet, J., and Allègre, C.J.: River dissolved and solid loads in the Lesser Antilles: new insight into basalt weathering processes. J. Geochem. Explor. 88, 308-312, doi: 10.1016/j.gexplo.2005.08.063, 2006.

Rupnik, E., Daakir, M., Deseilligny, M.P.: Open Geospatial Data, Software and Standards 2:14, doi:10.1186/s40965-017-0027, 2017.

Samper, A., Quidelleur, X., Lahitte, P., and Mollex, D.: 2007. Timing of effusive volcanism and collapse events within an oceanic arc island: Basse-Terre, Guadeloupe archipelago (Lesser Antilles Arc). Earth Planet. Sci. Lett. 258, 175–191, doi:10.1016/j.epsl.2007.03.030, 2007.

Seminara, G.: Fluvial sedimentary patterns, Annual Review of Fluid Mechanics, 42, 43–66, doi: 10.1146/annurev-fluid-121108-145612, 2010.

Seizilles, G., Lajeunesse, E., Devauchelle, O., and Bak, M.: Cross-stream diffusion in bedload transport, Phys. Fluids, 26, 013302, doi: 10.1063/1.4861001, 2014.

Shields, A. S.: Anwendung der Aehnlichkeitsmechanik und der Turbulenzforschung auf die Geschiebebewegung, Mitteilung der Preussischen Versuchsanstalt fur Wasserbau und Schiffbau, 26, 1936.

510   Summerfield, M. A., and Hulton, N. J.: Natural controls of fluvial denudation rates in major world drainage basins, J. Geophys. Res., 99(B7), 13871–13883, doi: 10.1029/94JB00715, 1994.

Terry, J.P., and Goff, J.: Megaclasts: proposed revised nomenclature at the coarse end of the Udden-Wentworth grain-size scale for sedimentary particles, Journal of Sedimentary Research, 84 (3): 192–197, doi: 10.2110/jsr.2014.19, 2014.

Thorne, P. D.: An overview of underwater sound generated by interparticle collisions and its application to the measurements
515   of coarse sediment bedload transport, Earth Surf. Dynam., 2, 531–543, doi: 10.5194/esurf-2-531-2014, 2014.

Turowski, J. M. and Rickenmann, D.: Tools and cover effects in bedload transport observations in the Pitzbach, Austria. Earth Surf. Process. Landforms, 34: 26-37. doi: 10.1002/esp.1686, 2009.

Wilcock, P. R. and McArdell, B. W.: Partial transport of a sand/gravel sediment. Water Resources Research, 33, 235-245, doi: 10.1029/96WR02672. 1997.

520   Wolman, M. G. and Miller, J. P.: Magnitude and frequency of forces in geomorphic processes, The Journal of Geology, 68, 54–74, 1960.

Yager, E. M., W.E. Dietrich, W.E., Kirchner, J.W., McArdell B.W.: Prediction of sediment transport in step-pool channels, WaterResour.Res., 48, W01541, doi:10.1029/2011WR010829, 2012.

19

525
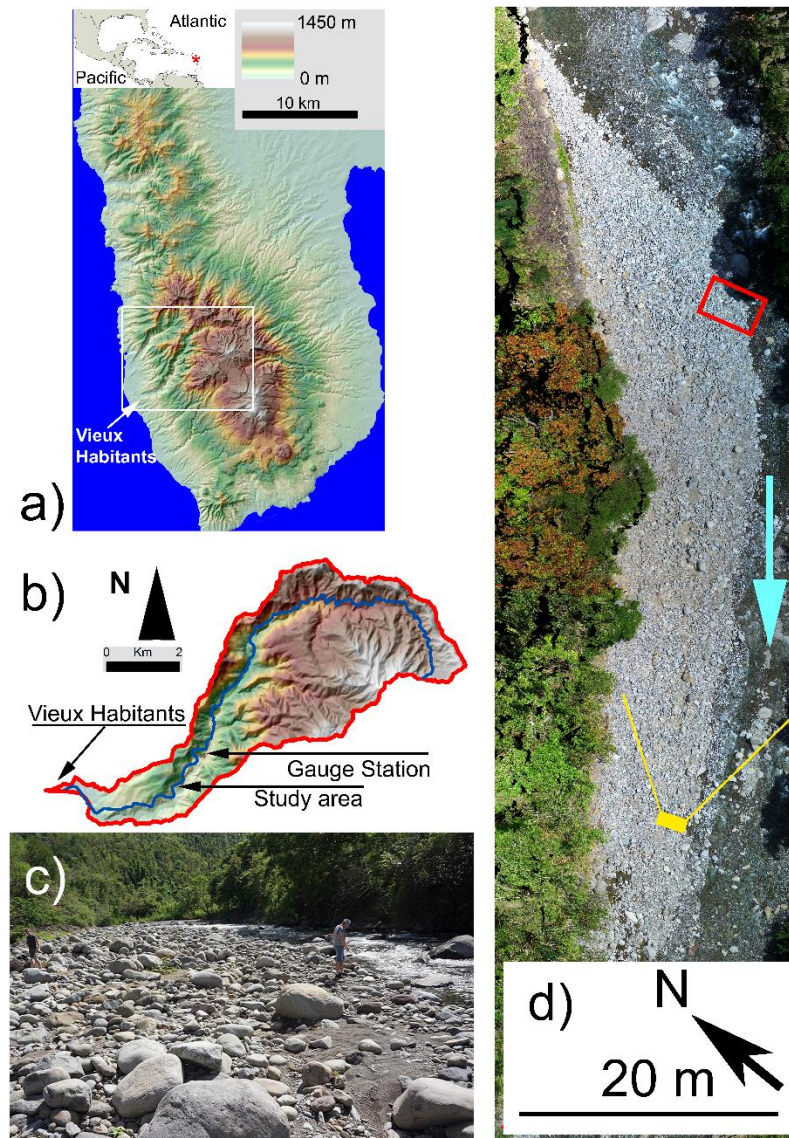
Figure 1: a) Basse Terre island in the Guadeloupe archipelago. The island separates the Atlantic Ocean in the East from the Caribbean Sea in the West. The white rectangle shows the position of the map displayed in b). b) ~~The~~Map of Vieux-~~Habitants river is located on the Caribbean side of Basse Terre. The watershed of Vieux Habitants has an area of 19 km².~~ ~~The length~~Habitant catchment, showing the course of the river ~~is 19 km. The water discharge is measured each 10 minutes at~~ (blue line). Two arrows indicate the positions of the Barthole

530 gauge station~~. The study area is located 2 km downstream of Barthole.~~ and of our field site. c) ~~A view~~Image of the bar taken from the ground, looking in the upstream ~~shows~~direction. Two persons visible on the image provide an approximate scale, from which the size of the boulders and their ~~heterometric~~ distribution~~. The two persons give the scale.~~ can be deduced. d) ~~The area of interest~~Aerial image of the bar, acquired with our UAV. The bar is about 300 m long and 15 to 35 m wide. It lies on the right side of the river 3 km upstream of the seashore. In fair weather conditions, the bar is bounded on its left by the channel of the river which is 5 to 10 m wide and less than 1 m deep. The boulder

535 bar is flooded 1 to 3 times a year. The red square shows the location of Fig. 3. The position of the camera and the field of view of c) is shown in yellow. ~~The flow direction is given by the~~ A turquoise arrow indicates the direction of the flow.
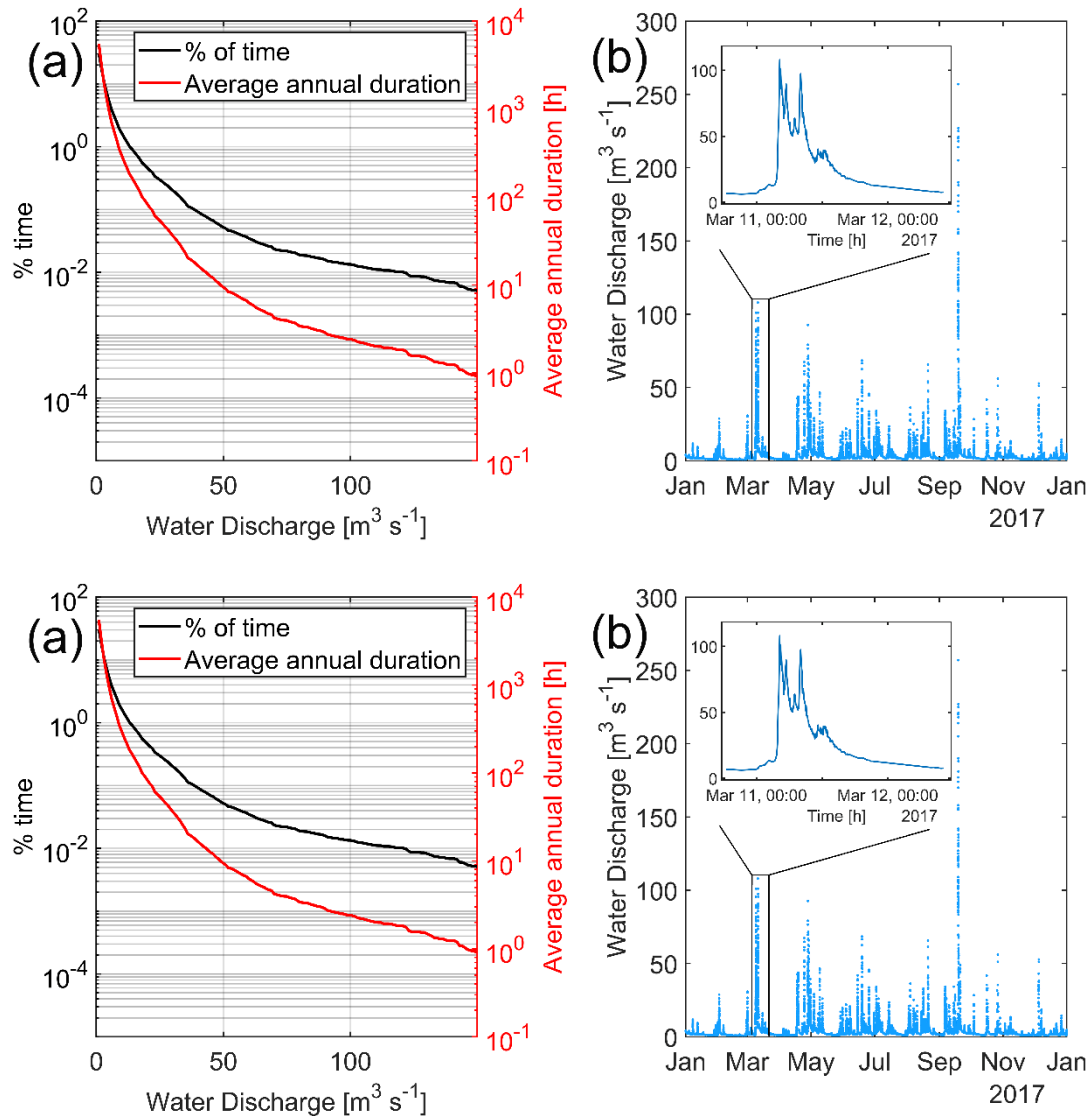
Figure 2: a) Percentage of time during which the ~~water discharge is~~ Vieux-Habitants river stays above a given ~~threshold based on data~~ discharge. This distribution is calculated from the data acquired between 2011 ~~to~~and 2018~~.~~ at the Barthole station. b) Hydrograph of the Vieux-Habitants river during the year 2017. ~~Most of the time, river is in low-flow conditions with less than 5 m³s⁻¹.~~ The ~~largest recorded~~ high peak in September 2017 corresponds to hurricane Maria, which struck Guadeloupe in September 19, 2017. During this hurricane, the discharge ~~was~~ reached up to 263 m³ s⁻¹. ~~It was reached on September 19 2017 during hurricane Maria. c) The inset shows a~~ Inset: typical flood~~. The water discharge reaches its maximum in less than one hour. The peak of the flow is followed by a slow recession.~~ event.

21
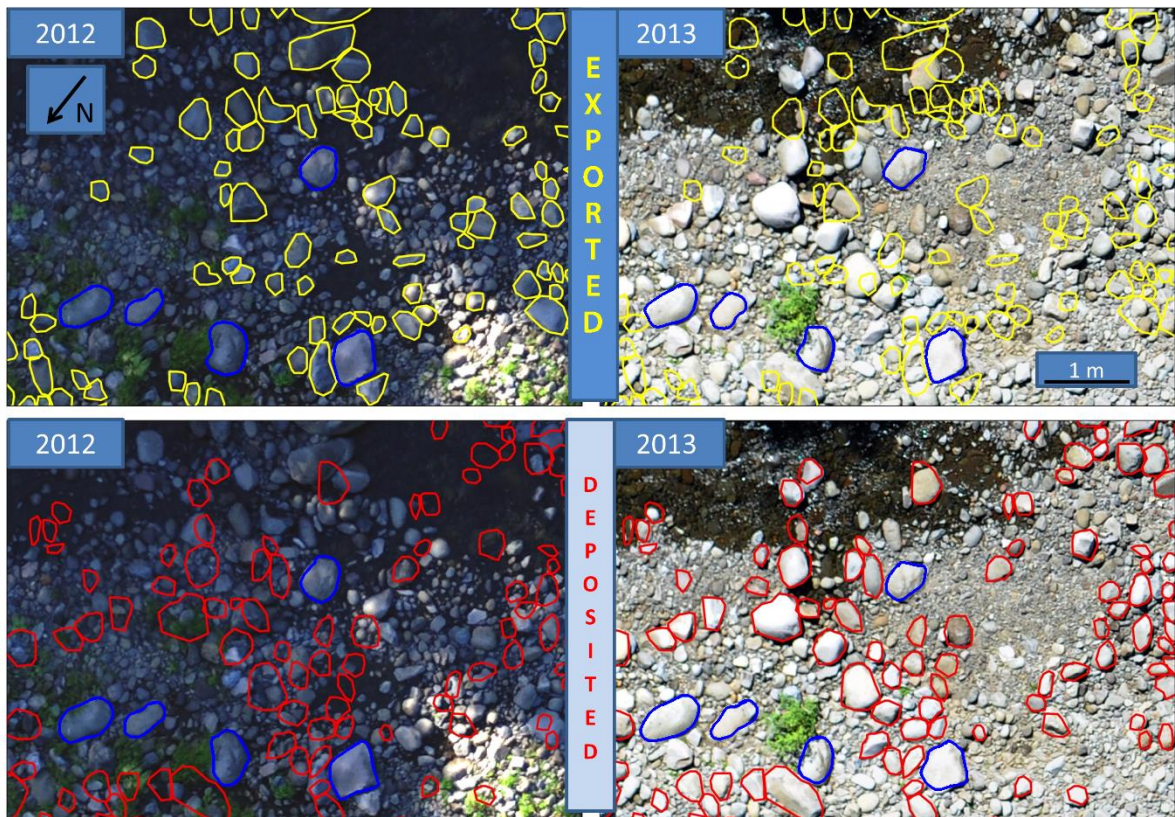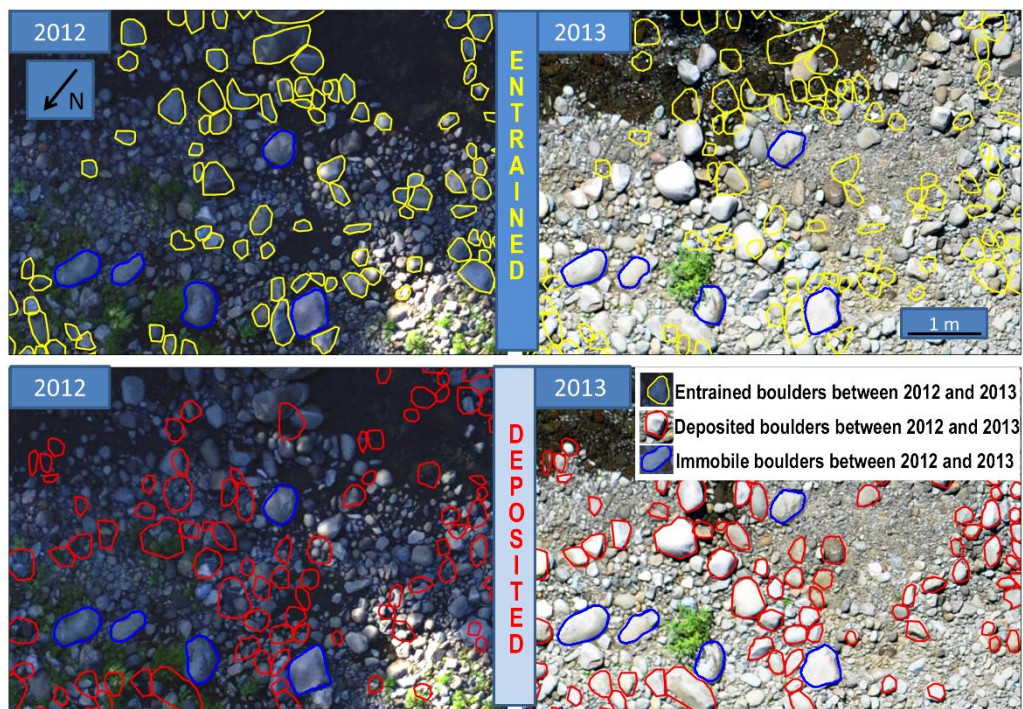
Figure 3: ~~Comparison between the surface~~ Surface of the bar in March 2012 (left) and June 2013 (right). ~~The upper pictures show the boulders that moved~~Boulders entrained by the river between 2012 and 2013~~. The~~ are marked by yellow contours (upper pictures). Boulders deposited by the river betwee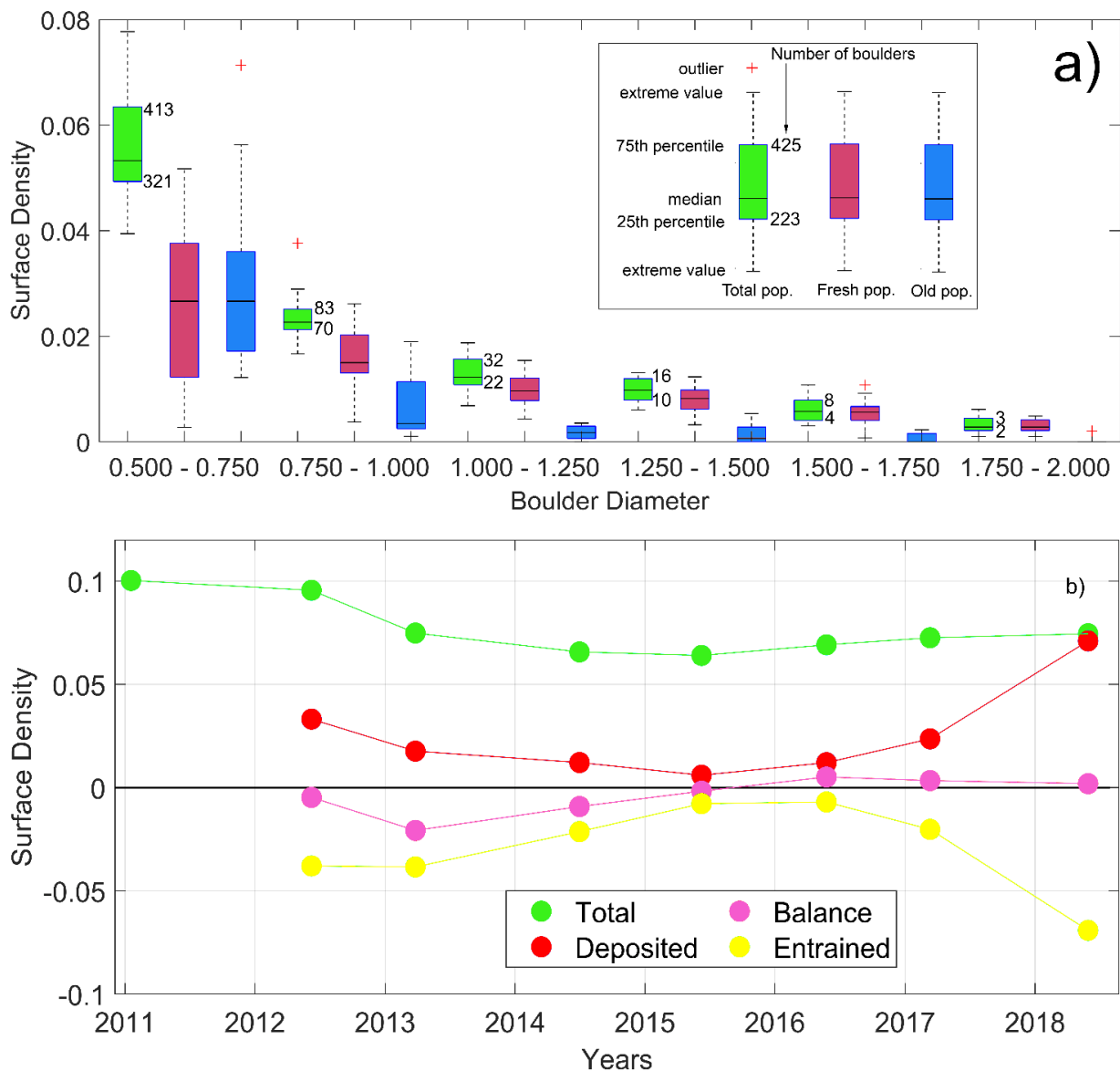n 2012 and 2013 are marked by red contours (~~lower pictures show the boulders that were deposited during the same period. Some boulders, outlined in~~). Boulders that stay in place between 2012 and 2013 are marked by blue~~, visible in 2012 are still there in 2013.~~ contours (lower and upper pictures).
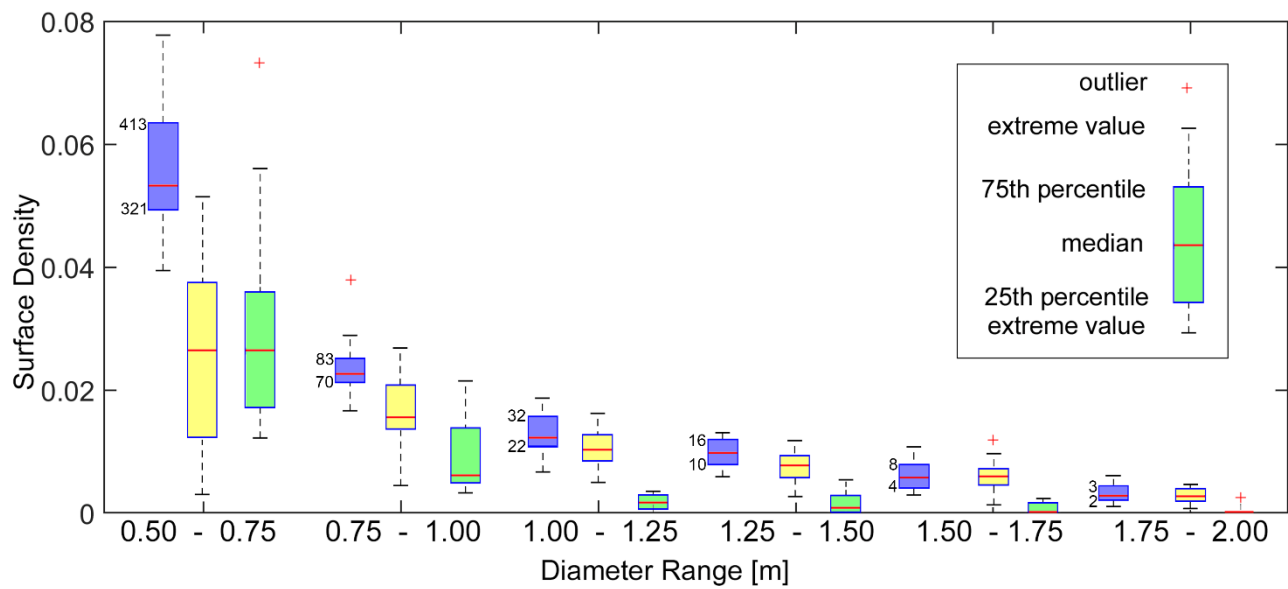
Figure 4a: a) Box plot of the surface ~~boulder~~ density of boulders (Eq. 1) ~~on~~at the surface the bar as a function of ~~the boulder~~their diameter, computed ~~for~~over the whole ~~duration of our~~ survey. ~~Blue~~Green: total number of boulders; ~~green~~red: freshly deposited boulders; ~~yellow~~green: boulders ~~that were~~ already in place during the ~~preceding~~previous campaign of observation.
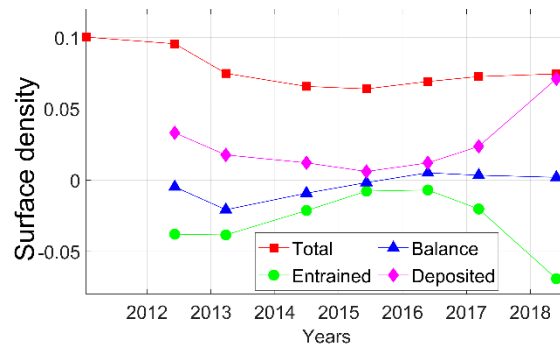
Figure 4b: b) Surface density of entrained, (yellow), deposited (red) and total (green) boulder population. Balance between deposited and entrained boulder population in pink. Data from 20102011 have been obtained from a preliminary campaign. Entrained boulders are counted negatively as they have been entrained out of the bar. Purple dots show the balance between entrained and deposited boulders.
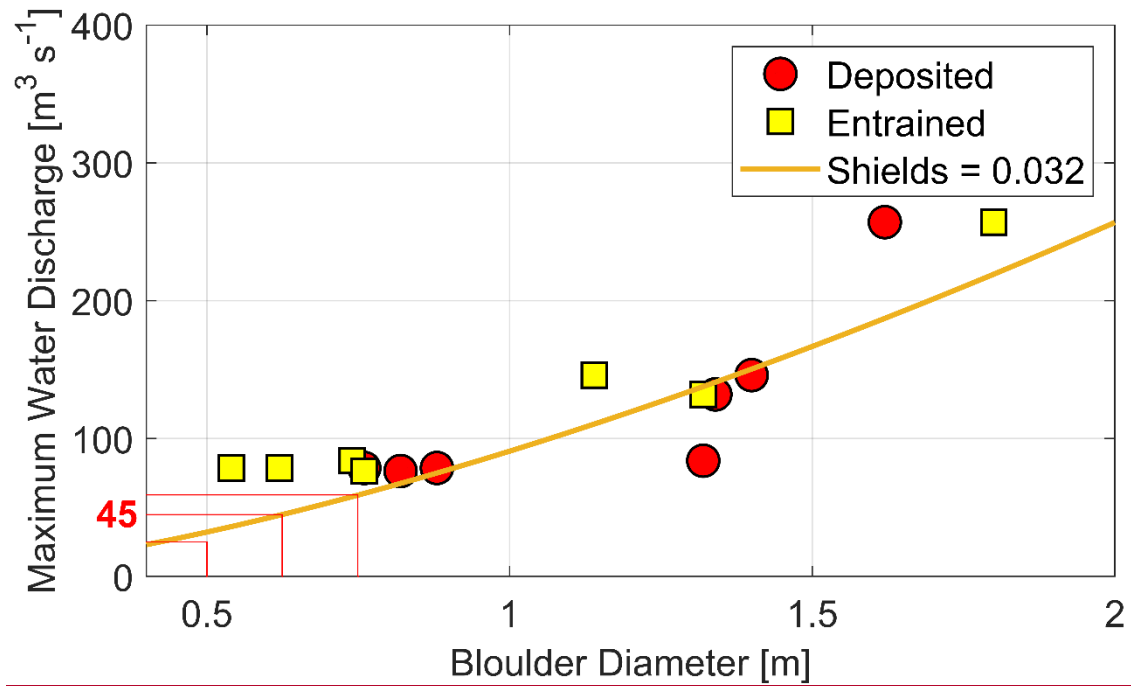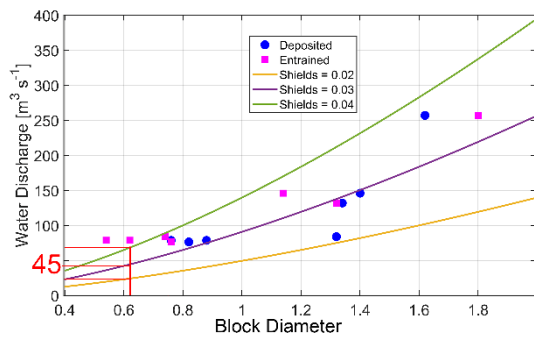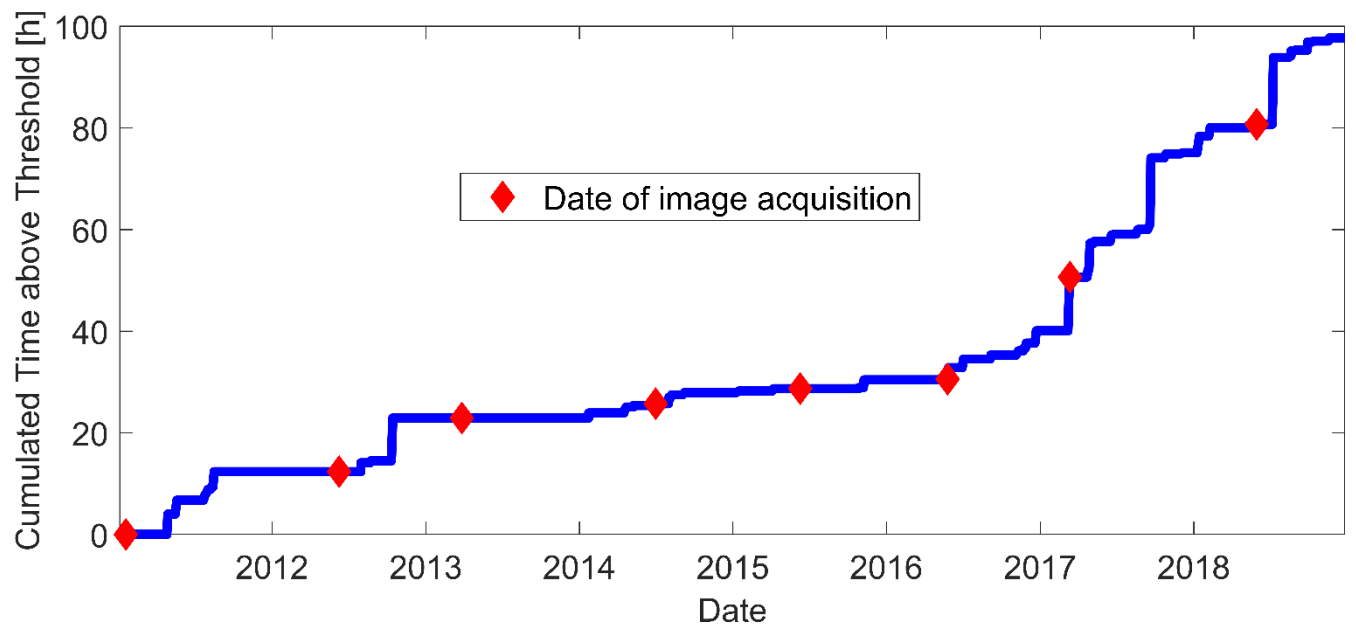
Figure 5: Maximum discharge recorded at the gauge station ~~between two consecutive campaigns~~ as a function of the size of the largest ~~transported~~ deposited (red dot) or entrained (yellow square) boulder. Orange line: fit of the data by Eq. (2).
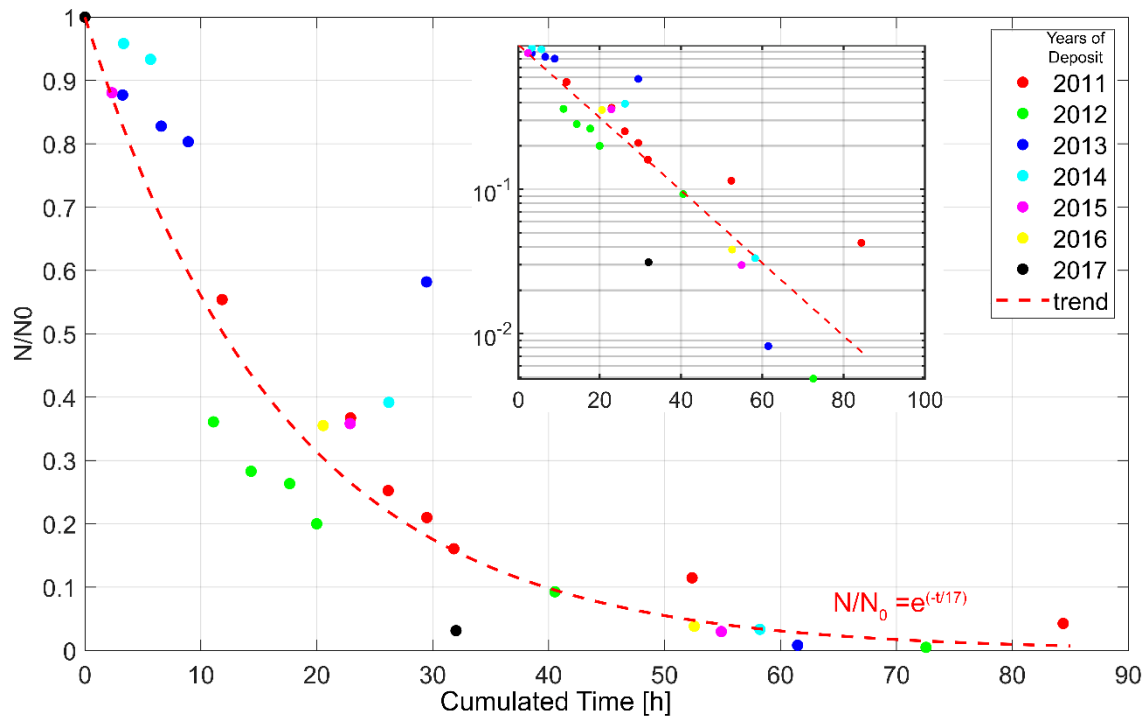
Figure 6: Effective transport time, i.e. cumulative time spent by the Vieux-Habitant river above the threshold discharge of 45 m^{3}s^{-1}.

Figure 7: ~~Population of~~ boulders ~~from 2011 to 2018. The curves represent the theoretical relation between water discharge and the maximum diameter of the exported or deposited boulders given by Eq. (2) (Appendix 1) for 3 values of Shields stress. The~~, normalized to its initial size, as a function of the cumulative effective transport time, calculated for a threshold discharge ~~for boulders with a diameter of 0.625 m~~ ranges from 24 to 69 $m^3 s^{-1}$ ~~According to the Shields stress. The parameters used for the theoretical estimation of the flow threshold are: Darcy-Weisbach friction coefficient C_f=0.1, critical Shield number Θ_c= 0.02-0.04, width of river, W=30 m, $\Delta\rho$ the density difference between grains and water 1900 kg m⁻³.~~
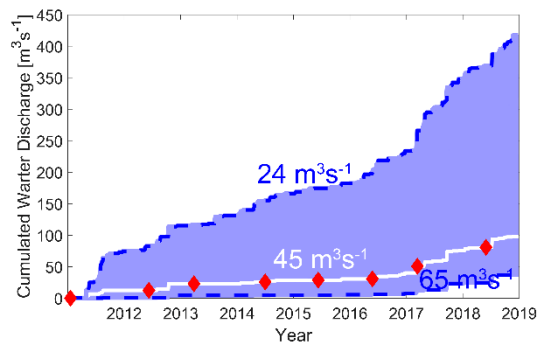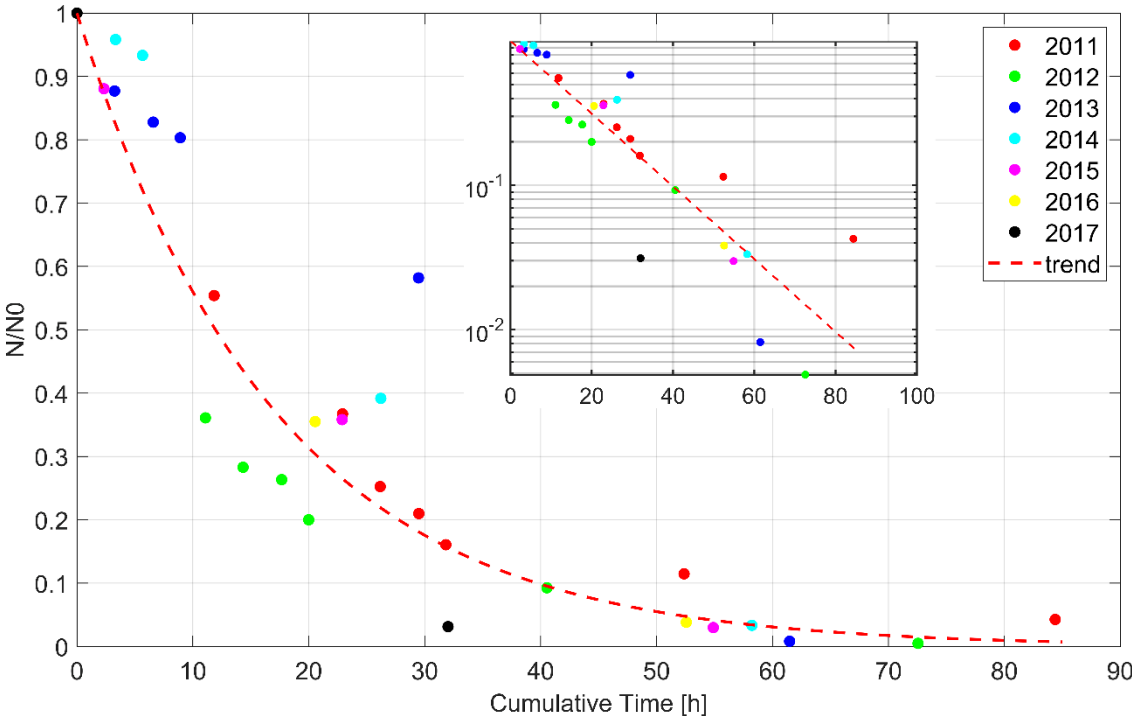
595   **Figure 7:** ~~Evolution of the number of boulders deposited on the bar between each campaign, and gradually entrained later. The horizontal axis is the transport time for a discharge threshold of 45 m³h⁻¹. The red~~of 45 m³ h⁻¹. The 7 populations of boulders that we monitor are plotted using different colors, as indicated on the plot. Red curve ~~is the best~~: fit of the data by Eq. 3 (exponential decay) with a residence time of 17h (half-life of 12 h). Inset: same ~~data in a~~plot with semi-logarithmic ~~scale~~axes.